Release of HIV-1 particles from the viral compartment in macrophages requires an associated cytoskeleton and is driven by mechanical constraints

Vasco Rodrigues[1], Sarah Taheraly[1], Mathieu Maurin[1], Mabel San-Roman[2], Emma Granier[1], Anaël Hanouna[1], Phillippe Benaroch[1]

1- Institut Curie, PSL Research University, INSERM U932, Paris, France
2- Institut Curie, UMR3215, Paris, France

Address correspondence to:

Vasco Rodrigues – vteixeir@curie.fr

Philippe Benaroch - Philippe.Benaroch@curie.fr

Abstract

A defining feature of HIV-1 replication in macrophages is that viral assembly occurs at the limiting membrane of a compartment often named VCC (virus-containing compartments) that is connected to the extracellular medium. The newly formed viral progeny pinches of the membrane and accumulates in the lumen of the VCC. While HIV budding has been extensively studied, very little is known about how viral particles present in the lumen of VCC are released in the extracellular medium. Here we show that the actin dynamics are critical for this process by combining ultrastructural analyses, time-lapse microscopy and perturbations of the actin cytoskeleton. We found that jasplakinolide, which stabilizes actin fibres, inhibited viral release from HIV-1-infected macrophages. Furthermore, in jasplakinolide-treated macrophages, VCC became scattered and no longer co-localized with the integrin CD18, nor the phosphorylated form of the focal adhesion kinase PYK2. Inhibition of PYK2 activity in infected macrophages promoted intracellular retention of viral particles in VCC that were no longer connected to the plasma membrane. Finally, we stimulated the rapid release of viral particles from the VCC by subjecting infected macrophages to frustrated phagocytosis. As macrophages spread on IgG-coated glass surfaces, VCC rapidly migrated to the basal membrane and released their viral content in the extracellular medium, which required their association with CD18 and the actin cytoskeleton. These results highlight that VCC trafficking and virus release are intimately linked to the reorganization of the macrophage actin cytoskeleton in response to external physical cues, suggesting that it might be regulated in tissues by the mechanical stress to which these cells are exposed.

35 **Introduction**

36 Macrophages are embedded in many tissues where they ensure specific functions. Early studies
37 established that HIV-1-infected patients possess infected macrophages in many of their tissues
38 (Orenstein et al., 1988). Usage of monocyte-derived macrophages (MDM) exposed to HIV-1 *in vitro*
39 allowed the study of the viral replication cycle and revealed some of its specific features as
40 compared to how it replicated in T lymphocytes (Rodrigues et al., 2017; Sattentau and Stevenson,
41 2016). Viral assembly takes place in macrophages at the limiting membrane of a compartment that
42 appears intracellular. The newly formed virions, pinch off from this membrane in the lumen of the
43 compartment, hence called VCC for virus-containing compartments, where they accumulate.
44 Interestingly, compartments with very similar characteristics are also present in uninfected
45 macrophages, as they similarly express tetraspanins (CD9, CD81 and CD53) (Deneka et al., 2007), and
46 the scavenger receptor CD36 (Berre et al., 2013). Upon HIV-1 infection, newly synthesized Gag is
47 recruited to these pre-existing compartments that become *de facto* VCC (Berre *et al.*, 2013).

48 The VCC possess a very intricate architecture and are often connected to the extracellular medium
49 by channels or conduits that are too narrow to allow the virions to exit but that permit fluid
50 exchanges (Gaudin et al., 2013; Welsch et al., 2007). They remain mostly inaccessible to
51 macromolecules delivered from the extracellular media, such as antibodies (Chu et al., 2012). The
52 precise nature of the VCC has been debated but the current view holds that it originates from
53 tetraspanin-rich zones of the plasma membrane that have been internally sequestered. While VCC
54 are generally considered as continuous with the plasma membrane, recent work also evidenced the
55 presence of completely enclosed compartments that could fuse with plasma membrane-connected
56 compartments (Ladinsky et al., 2019). These studies highlight a rather complex and dynamic
57 structure that results in a more complex release of viral particles as compared with other cell types.

58 How the virions stocked in the VCC lumen are released in the extracellular medium remains an open
59 question. To our knowledge, a single study reported that the release of viral particles from the VCC
60 can be induced. Exposure of an infected MDM to extracellular ATP (eATP) prompted a rapid
61 discharge of the viral particles stored in the VCC, via stimulation of the P2X7 purinergic receptor
62 (Graziano et al., 2015). The rapid and drastic remodelling of the cell shape and actin cytoskeleton
63 that eATP induces on HIV-infected MDMs may underlie its impact on viral release. This
64 interpretation raises the question of how the structure of the VCC, their trafficking, and
65 consequently viral particle release are impacted by or depend on the actin cytoskeleton.

66 The VCC are surrounded by a meshwork of filamentous actin tightly associated with its external
67 membrane (Mlcochova et al., 2013; Pelchen-Matthews et al., 2012), which is often decorated by an

68 electron dense molecular coat that appears to anchor the actin cytoskeleton to the compartment
69 (Pelchen-Matthews *et al.*, 2012). These coats have striking resemblances with focal adhesions, as
70 they contain the ß2-integrin CD18 and its associated CD11b and CD11c α-integrins. Focal adhesion
71 linker proteins, such as talin, vinculin and paxillin are also found at these molecular coats (Pelchen-
72 Matthews *et al.*, 2012). Silencing CD18 in HIV-1 infected macrophages, did not alter viral release
73 over a 24-hour window. Whether a longer period of analysis impacts viral release was not assessed;
74 nevertheless, CD18 silencing led to scattering of the VCC across the cell (Pelchen-Matthews *et al.*,
75 2012), suggesting that these coats are an integral part of the compartment.

76 In macrophages, many focal adhesion-mediated processes such as cell migration are regulated by
77 Focal Adhesion Kinase (FAK)-related proline-rich tyrosine kinase 2 (PYK2) (Okigaki et al., 2003). PYK2
78 promotes the assembly of focal adhesions at the leading edge, and their disassembly at the trailing
79 edge to ensure net forward movement (Zhu et al., 2018). The full breadth of PYK2 activators and
80 substrates remain incompletely understood, but it is generally considered to act at the cross-roads
81 between integrin and small GTPases, such as Rho (Schaller, 2010).

82 It remains unclear how the VCC structure and HIV particle release are impacted by these focal
83 adhesion-like coats and PYK2 signalling and, in general, our understanding on how the actin
84 cytoskeleton impacts HIV release from macrophages remains rudimentary. We report here that
85 pharmacological stabilization of actin fibres led to scattering of the VCC and impeded viral particle
86 release from infected MDM. This was paralleled by decreased association of the integrin CD18 and
87 of the phosphorylated form of the kinase PYK2 with the compartment. Specific inhibition of PYK2 led
88 to accumulation of viral particles in VCC that lost connection to the plasma membrane. Finally,
89 subjecting infected MDM to frustrated phagocytosis on glass coverslip induced rapid trafficking of
90 VCC to the surface and viral release. Such trafficking required the compartment to be associated
91 with CD18 and the actin cytoskeleton. We propose that focal adhesion-like coats are regulated by
92 PYK2 and anchor the actin cytoskeleton to the VCC to promote HIV release from macrophages.

93 **Results**

94 **1. Actin dynamics modulates viral particle release from HIV-1-infected macrophages**

95 In MDMs infected with HIV-1-GAG-iGFP-ΔENV-VSVG for 4 days, phalloidin staining can be readily
96 observed around the VCC, confirming previous observations (Mlcochova *et al.*, 2013) (Fig. 1A-B). F-
97 Actin appears docked at or surrounding the compartment (see 3D inset in Fig. 1B). Ultrastructural
98 analysis by electron microscopy (EM) revealed the presence of actin filaments anchored at and
99 radiating from the VCC (Fig. S1A-B). Live imaging of MDMs transduced with Lifeact-mCherry and
100 infected with HIV-1-GAG-iGFP-ΔEnv-VSVG confirmed that the VCC and the actin cytoskeleton are in
101 proximity to each other, and exhibit synchronized movements (Fig. 1C and Video S1).

102 To explore how the actin cytoskeleton may impact on the structure of the VCC and viral release, we
103 first employed a cell micropatterning technique to physically manipulate the actin cytoskeleton
104 organization in HIV-1-infected MDMs (Fig. S2A-S2B). Indeed, adherent cells adapt to the
105 micropattern shape by remodelling their actin cytoskeleton as to maximize adhesion (Thery, 2010).
106 We observed that plating HIV-1-infected MDMs on distinct micropatterns impacted on the total
107 volume of the VCC (Fig. S2A-S2B). This was particularly evident in crossbow-shaped macrophages,
108 which presented stress fibres at the non-adherent edges, and bore significantly smaller VCCs (Fig.
109 S2A-S2B). Nonetheless, these cells did not remain immobile over the patterned areas for prolonged
110 periods of time, precluding any accurate analysis on viral particle release. We turned thus into
111 pharmacological manipulation of the actin cytoskeleton of infected macrophages to ascertain how it
112 impacts on the VCC size and structure as well as viral release.

113 We infected MDMs with HIV-1-ΔENV-VSVG for 4 days to allow formation of VCCs and treated them
114 with a panel of pharmacological modulators of the actin cytoskeleton. Over the next 24 hours, we
115 observed that the F-actin stabilizing drug, jasplakinolide, reduced the release of viral particles (Fig.
116 1D), as measured by our in-house CBA assay that specifically detects the HIV-1 p24 capsid protein
117 (Fig. S3A). None of the other cytoskeleton-modifying drugs had significant effects on viral release
118 over the 24 hours period (Fig. 1D). Jasplakinolide was also the sole drug to induce retention of p24
119 inside the macrophage during the 24 hours treatment period, suggesting that the viral particles are
120 retained inside the cell, hence their decreased concentration in the supernatant (Fig. 1E-G).
121 Interestingly, treatment of HIV-1-infected HeLa cells with the same cytoskeleton modulators failed
122 to induce any significant changes in p24 release over vehicle-treated cells (Fig. S3B), suggesting that
123 the effect of jasplakinolide treatment implicates the VCC, a macrophage-specific structure.

124

125 **2. Stabilization of actin fibres impacts VCC structure and architecture**

126 We next asked how jasplakinolide treatment results in retention of p24 in the macrophage, by
127 examining its impact on the VCC by confocal microscopy. MDMs were infected with HIV-1-GAG-iGFP-
128 ΔENV-VSVG for 4 days, treated or not with a non-toxic dose of jasplakinolide for 24 hours and
129 analysed by confocal microscopy. As expected, the drug had a strong impact on the general
130 macrophage morphology, as cells rounded up and lost their typical spreading over the substrate (Fig.
131 2A). While this led to a significant decrease in cell spreading (Fig. 2B), treatment with jasplakinolide
132 increased the total volume of the VCC by more than 2-fold (Fig. 2C). The average intensity of the
133 Gag-iGFP signal was similar between treated and not treated cells (Fig. 2D), although the
134 compartment spread more evenly throughout the cell (Fig. 2E). These observations were confirmed
135 by EM, as the typical VCC in vehicle-treated cells appear to fragment into smaller, but more
136 numerous, compartments after treatment with jasplakinolide (Fig. 2F). Jasplakinolide-treated MDMs
137 also exhibited massive accumulations of F-actin that occupied large sections of the cytoplasm (Fig.
138 2G, bottom left panel). Their appearance is concomitant with loss of the actin filaments that typically
139 radiate from the VCC in control macrophages. Overall, these data suggest that drug-induced F-actin
140 stabilization leads to loss of the organized actin filaments that are anchored at the VCC.
141 Consequentially, compartments become dispersed throughout the cell and accumulate, resulting in
142 impaired viral release.

143

144 **3. Stabilization of actin fibres relocalizes the integrin CD18 away from the VCC-limiting membrane**

145 Previous work reported that the β2-integrin CD18 is present in focal adhesion-like electron dense
146 regions at the limiting membrane of the VCC and is critical for the integrity of the VCC (Pelchen-
147 Matthews *et al.*, 2012). We confirmed the presence of electron dense regions that coat the VCC and
148 that serve as anchoring sites for the actin cytoskeleton (Fig. 3A, Fig. 2G and Fig. S1A-B). These coats
149 were also present in VCCs at, or close to, the cell surface (Fig. 3B), suggesting their implication on the
150 trafficking of the compartment. Confocal immunofluorescence confirmed that CD18 surrounds the
151 VCC (Fig. 3C-D). However, treatment with jasplakinolide lead to a significant decrease on the
152 enrichment of CD18 at the vicinity of the VCC (Fig. 3C-D). Analysis by EM confirmed that the electron
153 dense coats typical of control MDMs, were no longer observable in the smaller and more numerous
154 VCCs of jasplakinolide-treated cells (Fig. 3E-F and Fig 2G). Our data indicates that pharmacological
155 stabilization of actin leads VCCs to lose their association with focal adhesion-like coats and the
156 integrin CD18, which possibly underlies the accumulation of viral particles inside the cell.

157

158 **4. The phosphorylated form of the focal adhesion kinase PYK2 localizes at the VCC**

159 Because of the similarities between focal adhesions and the electron dense coats around the VCC,
160 we evaluated whether PYK2, a non-receptor tyrosine focal adhesion kinase (FAK) that governs the
161 focal adhesion response to integrin-mediated signalling, plays a role on the VCC structure and HIV-1
162 release from macrophages. A 4-day infection of MDMs with HIV-1-ΔENV-VSVG led to activation of
163 PYK2, as evidenced by an increase in the levels of phosphorylated PYK2 at Tyr402 (Fig. 4A), in
164 agreement with a previous report (Del Corno et al., 2001). Confocal microscopy revealed that P-PYK2
165 (Y402) localized mostly to the basal surface of the macrophage and was organized into large clusters
166 that likely corresponded to podosomes (Fig. 4B). Yet, a small pool of P-PYK2 located at the VCC in
167 DMSO-treated cells (Fig. 4B). While jasplakinolide treatment had no effect on the global levels of
168 PYK2 Tyr 402-phosphorylation induced by HIV-1 infection (Fig. 4A), it led to loss of the enrichment of
169 P-PYK2 at the VCC observed in vehicle-treated cells, as the P-PYK2 signal dispersed evenly
170 throughout the cell (Fig. 4B-C). These data indicates that jasplakinolide treatment induces loss of
171 association of the phosphorylated form of PYK2 from the VCC, accompanying the loss of CD18 and
172 focal adhesion-like coats.

173

174 **5. Active PYK2 participates in viral particle release from the VCC**

175 Overall, our results hint at a possible role for PYK2 as coordinating actin dynamics at the VCC, since
176 (1) its active phosphorylated form localizes to the compartment, and (2) jasplakinolide treatment
177 disrupts its localization at the VCC, concomitant with loss of the electron dense regions and CD18
178 expression at the compartment. To directly test this hypothesis, we treated HIV-1-ΔENV-infected
179 MDMs with PF431396 (PF396), a dual FAK/PYK2 inhibitor that has higher affinity for PYK2 over FAK
180 (IC50 values of 2 and 11 nM, respectively). PF396 prevented the phosphorylation of PYK2 induced by
181 HIV-1 infection and decreased p24 release from infected macrophages, over a 96-hour period and,
182 conversely, promoted its retention inside the cell (Fig. 5A-C). We next examined the VCCs of
183 macrophages infected with HIV-1 GAG-iGFP-ΔENV-VSVG for 4 days and treated for additional 4 days
184 with PF396 (Fig. 5D). While PF396 had no evident impact on the macrophage morphology, including
185 cell volume (Fig 5E), it led to a significant increase in the compartment volume (from 42.26 μm^3 in
186 DMSO-treated cells to 103.13 μm^3 in PF396-treated cells) (Fig. 5F), without an impact on the mean
187 intensity of the Gag-iGFP signal (Fig. 5G). These VCC from PF396-treated MDMs often had a granular
188 or reticulated appearance (Fig. 5D and S4A). While F-actin remained localized close to the
189 compartment in PF396-treated cells, it appeared evenly distributed throughout the VCC, rather than
190 being concentrated as patches in one side, as commonly observed in vehicle-treated cells (Fig 5D).
191 Despite their larger volume, VCC from PF396 treated cells were more compact, as revealed by their

192 decreased spreading scores (Fig 5H). Finally, while CD18 remained enriched in the vicinity of the VCC
193 after PF396 treatment, its distribution was more even, as observed with F-actin (Fig. 5I and Fig. S4A).

194 Due to the increased compactness of VCC from PF396-treated macrophages, we hypothesized that
195 the VCC continuity with the plasma membrane may be altered after exposure to the drug, which
196 could explain the decreased viral particle release. We thus exposed PF396-treated or vehicle-treated
197 macrophages to CellBrite®, a non-permeable lipophilic dye that can withstand fixation. Strikingly, we
198 observed strong accumulation of the dye in VCC from DMSO-treated macrophages, while those from
199 PF396-treated cells were generally negative for CellBrite staining (Fig. 5J-L and Fig. S5A). Finally,
200 PF396 treatment did not render VCC accessible to an anti-CD44 antibody added from the
201 extracellular media (Fig. S6A), although VCC from PF396-treated cells could still be stained with anti-
202 CD44 after cell permeabilization (Fig. S6B). PYK2 is known for its critical role in regulating actin
203 dynamics at focal adhesions (Schaller, 2010). Our data suggest that it is endowed with a similar role
204 at the VCC, promoting its trafficking to the surface and regulating its connectivity to the plasma
205 membrane.

206

207 **6. Frustrated phagocytosis of HIV-1-infected MDM induces the rapid release of viral particles from**
208 **VCC**

209 While our previous experiments have examined the role of the actin cytoskeleton in regulating HIV
210 release from resting macrophages, we aimed to observe its impact in cells undergoing a dynamic
211 process. For that, we subjected HIV-1-infected MDMs to frustrated phagocytosis. In this
212 experimental system, macrophages spread rapidly on the substrate, driven by actin polymerization
213 that promotes a fast and concentric extension of pseudopods, until the plasma membrane tension
214 increases to a point that no longer allows further spreading (Masters et al., 2013). If an HIV-1-
215 infected macrophage is subjected to frustrated phagocytosis, we hypothesize that VCC act as
216 membrane reservoirs that can be deployed rapidly to the surface to counteract the increase in
217 plasma membrane tension, and that their anchoring to the cytoskeleton would be required for such
218 rapid deployment. We thus seeded MDMs, infected for 3 days with HIV-1-GAG-iGFP-ΔENV-VSVG,
219 over a human IgG-coated surface and performed live imaging. As exemplified in Fig. 6A, the
220 macrophage spread rapidly on the surface with its projected area more than doubling in 20 minutes
221 (Fig. 6A-B and Video S2). We further observed a steady decrease in the volume of the VCC starting at
222 around 8 minutes (Fig 6A and 6B). The compartment appears to migrate towards the basal surface,
223 as the cell spreads, where its intensity decreases, presumably due to virion release (Fig. 6A, xz
224 planes). Indeed, by quantifying the amount of p24 in the culture supernatant, we observed a rapid

225 release of the capsid protein from MDMs seeded over IgG-coated coverslips as compared with
226 control coverslips or control coverslips + IgG added at the same time as the cells ("Soluble IgG") (Fig.
227 6C), during the first two hours. Such rapid kinetics suggests that it is the preformed viral particles
228 stored in VCCs that are released during frustrated phagocytosis and not a general increase in viral
229 production due to macrophage activation. Supporting this idea, at later time-points there were no
230 differences in the concentration of p24 released from macrophages seeded in the three different
231 conditions (Fig. 6C). Thus, as macrophages spread during frustrated phagocytosis, VCC appear to be
232 pulled to the basal surface of the cell, where they release their contents.

233 We next tested whether the actin cytoskeleton participates in VCC trafficking during frustrated
234 phagocytosis. We fixed HIV-1-infected MDMs subjected to frustrated phagocytosis or in control
235 conditions and examined by confocal microscopy (Fig. 6D). In cells under frustrated phagocytosis, F-
236 actin concentrated on the protruding edges and as expected, these cells spread over the glass
237 surface (Fig. 6E). The VCC were significantly reduced in their volume in cells undergoing frustrated
238 phagocytosis (Fig. 6F), as was the mean intensity of the Gag-iGFP signal (Fig. 6G). Interestingly, the
239 remaining VCC in MDMs under frustrated phagocytosis were mostly devoid of associated F-actin
240 (Fig. 6D). Furthermore, while VCC from control MDMs were associated with CD18, as expected, after
241 frustrated phagocytosis the remaining VCCs lost this association (Fig. 6H and Fig. S7A). Finally,
242 P(Y402)-PYK2 concentrated mostly in the protruding edges in cells under frustrated phagocytosis,
243 while remaining VCC in general lacked P-PYK2 (Fig. S7B). This strongly suggests that the rapid
244 deployment of the VCCs to the surface that occurs during frustrated phagocytosis, requires an
245 associated cytoskeleton and focal adhesion-like coats, and that compartments lacking such
246 associated complexes remain inside the macrophage after frustrated phagocytosis.

247

248 **Discussion**

249 Overall, our data highlights the importance of the actin cytoskeleton and associated factors in
250 regulating the release of HIV-1 from its VCC in macrophages, likely by providing a physical anchor
251 that promotes its movement, connectivity with the plasma membrane and, consequentially, viral
252 release. While previous studies addressed the presence of an actin cytoskeleton associated with the
253 VCC, and its importance for viral release, the molecular details remained unknown. Here, we
254 uncover an important role for the CD18-PYK2 axis as modulators of the VCC structure, its trafficking
255 dynamics and viral release.

256 Cell shape is governed by the actin cytoskeleton, particularly cortical actin (Chalut and Paluch, 2016).
257 To start exploring the importance of the actin cytoskeleton on HIV release from macrophages, we
258 developed a micropatterning technique for HIV-1-infected macrophages. Our data indicates that the
259 VCC's structure and size are sensitive to cell shape. Particularly, macrophage adhesion to the
260 crossbow pattern imposes strong physical constraints resulting in smaller VCC that are mostly devoid
261 of surrounding F-actin. Accurate estimation of viral particle release was not achievable due to the
262 strong adhesive properties of macrophages which tended to invade the surrounding anti-adhesive
263 PEG-based substrate after a few hours of seeding over patterns. Nevertheless, our finding that PEG-
264 Silane can, at least temporarily, efficiently micropattern primary human MDMs, may serve as a
265 useful tool for future studies employing micropatterning to study human macrophage biology.

266 By exposing infected MDMs to different pharmacologic modulators of the cytoskeleton we found
267 that the F-actin stabilizing drug jasplakinolide significantly impacted on viral release to the
268 supernatant. A previous report demonstrated an increase in viral release from HIV-1-infected
269 macrophages after treatment with the actin depolymerizing drug latrunculin, or the actin
270 polymerization inhibitors, cytochalasin E or D (Mlcochova *et al.*, 2013). In our hands, the actin
271 depolymerizing drug mycalolide B had no significant effect on viral release over a 24-hour period.
272 Differences in the viral strains employed, experimental conditions or the distinct mechanisms
273 through which mycalolide B and latrunculin depolymerize actin (Hayashi-Takanaka et al., 2019), may
274 account for the divergent results.

275 The ARP2/3 complex inhibitor CK666 had no effect in viral release over 24 hours. Longer exposure to
276 CK666 led to toxic effects, so we cannot exclude that in the long-term actin polymerization may be
277 required for viral release. Nevertheless, at least in the short term, actin polymerization may not be
278 necessary for HIV release from macrophages. Similarly, the myosin II inhibitor blebbistatin had no
279 significant effect on viral release over a 24-hour period, suggesting that actomyosin contraction is
280 not a major driver of viral release, at the steady state.

281 The use of pharmacological manipulation of the actin cytoskeleton is not without its shortcomings,
282 due to its critical importance in multiple other biological processes. During HIV infection actin
283 impacts virtually on every step of the viral cycle (Ospina Stella and Turville, 2018). To minimize "off-
284 target" effects, we allowed the establishment of the infection and formation of VCCs for 4 days
285 before addition of the cytoskeleton modulators, as to exclude any effect on the early steps of the
286 viral cycle. Nevertheless, we can't dismiss certain unwanted effects may indirectly impact on HIV
287 release.

288 Jasplakinolide treatment had no effect on p24 release from infected HeLa cells. Previous work
289 showed that while latrunculin augmented viral release from macrophages, it had no effect on
290 infected HEK 293 cells (Mlcochova *et al.*, 2013). Given that in these cell lines HIV-1 viral particles
291 directly bud to the extracellular media, their release may not be impacted by modulating actin
292 dynamics. Nevertheless, studies addressing the impact of viral release from non-macrophage cells
293 often yielded inconsistent results (Ospina Stella and Turville, 2018). Some reports suggest that actin
294 may be important for the assembly and budding processes (Thomas et al., 2015; Wen et al., 2014),
295 but this is at odds with a study that tracked individual budding sites in real-time in HeLa cells,
296 demonstrating that assembly and budding proceed unimpaired even after total depolymerization of
297 actin (Rahman et al., 2014). Thus, it will be important to standardize experimental approaches to
298 study the effects of the actin cytoskeleton on HIV assembly and budding. In macrophages, the field
299 will face the added challenge of discriminating between the impact of actin modulation on viral
300 assembly and budding, and its influence on VCC trafficking, as both may impact on viral release.

301 In HIV-infected macrophages exposed to jasplakinolide, VCC scattered throughout the cell and were
302 smaller, but more numerous, such that their total volume increased. They were devoid of associated
303 actin, CD18 and the focal adhesion-like coats typically found in non-treated infected cells. In non-
304 treated and infected macrophages, we observed that actin bundles frequently radiated from these
305 VCC coats, suggesting that they are the site of anchoring of the cytoskeleton to the compartment.
306 Jasplakinolide induces the loss of these structures, concomitant with the fragmentation of the
307 compartment, suggesting an important role for the coats and their associated cytoskeleton in
308 maintaining the integrity of the VCC.

309 Our frustrated phagocytosis assays indicate an important role for the actin cytoskeleton and VCC-
310 associated CD18 in the trafficking of the compartment to the surface. We show that the drastic
311 remodelling of the macrophage morphology that occurs in frustrated phagocytosis leads to rapid
312 viral release, associated with loss of VCCs. Importantly, those VCC remaining in the cell after
313 frustrated phagocytosis were small and mostly devoid of actin and CD18, suggesting that these are
314 required for rapid VCC trafficking to the surface and viral release. VCC appear to be pulled rapidly to

315 the basal surface of the cell during frustrated phagocytosis. Is the pulling force transmitted through
316 the actin bundles connected to the compartment, as our observations suggest? If yes, where does
317 such force originate from, and what is the role of the electron dense coats that surround the VCC?
318 One may speculate that the coats act as traction points, upon which pulling forces may act, in a
319 manner akin to focal adhesions during mesenchymal cell migration (Bear and Haugh, 2014). In this
320 scenario, one would expect a role for actomyosin contraction at the origin of the pulling forces
321 acting on the VCC. While we failed to observe any effect of myosin II inhibition in viral release from
322 macrophages at the steady state, its impact may be more prominent during an event such as
323 frustrated phagocytosis, where VCCs rapidly traffic through the cell. However, given the known role
324 for myosin II in the formation of phagocytic cups, we could not test the impact of its inhibition in
325 viral release during frustrated phagocytosis (Olazabal et al., 2002). Future studies, employing
326 alternative approaches able to specifically isolate the role of myosin II in VCC trafficking could help
327 answer this question.

328 We found that the phosphorylated form of the kinase PYK2 localizes at the VCC, and that
329 jasplakinolide treatment redistributes it throughout the cell. The key role this kinase plays in
330 regulating the dynamics of focal adhesions in macrophages, prompted us to explore its importance
331 in HIV release. Inhibiting PYK2 led to viral particle accumulation in the macrophage, associated with
332 larger VCC that often had a granular appearance. While F-actin and CD18 associated with the VCC via
333 patches or focal points in control cells, treatment with the PYK2 inhibitor led to a more even
334 distribution of these factors on the compartment. This suggests that PYK2 inhibition leads to altered
335 organization of the focal adhesion-like coats that attach the actin cytoskeleton to the VCC, which
336 may possibly underlie its impact on viral release. PYK2 inhibition also led VCC to lose plasma
337 membrane connectivity, concomitant with the increased compaction of the compartment and
338 perinuclear location. In vehicle-treated and infected cells, certain VCC were connected to the plasma
339 membrane, while others not, in agreement with previous observations (Deneka *et al.*, 2007; Gaudin
340 *et al.*, 2013). In bone marrow macrophages from humanized mice infected with HIV-1, completely
341 enclosed compartments were often perceived, and these occasionally fused with plasma membrane-
342 connected compartments (Ladinsky *et al.*, 2019). Integrating these observations with our new data,
343 VCC appear to alternate between enclosed and plasma membrane-connected states, in a manner
344 regulated by PYK2 activity. These enclosed compartments maintain the expression of VCC classical
345 markers such as CD18 and CD44, despite remaining inaccessible to antibodies added prior to cell
346 fixation and permeabilization.

347 PYK2 phosphorylation has been previously reported during HIV-1 infection and occurs downstream
348 of co-receptor engagement by the envelope glycoprotein gp120 (Del Corno *et al.*, 2001), but not

349 when Δ*Env,* pseudotyped viruses are used (Davis et al., 1997). Thus, our data points to a distinct,
350 lasting, activation of PYK2 during HIV-1 infection mediated by an undescribed mechanism. In
351 macrophages, HIV can reprogram cell migration, via its accessory protein Nef, towards a
352 mesenchymal mode (Verollet et al., 2015), which depends on adhesive structures such as
353 podosomes (Van Goethem et al., 2010) and is associated with PYK2 activation (Duong and Rodan,
354 2000). It is thus possible that a later activation of PYK2 by HIV Nef may contribute to enhancing viral
355 release from macrophages.

356 A limitation of our study that could be explored in future research was the use of *Env*-deficient
357 viruses pseudotyped with VSV-G to achieve single-cycle infections. This strategy avoids propagation
358 of the infection, which could indirectly impact the quantification of viral release. However, in our
359 cultures, direct viral transmission from one cell to another does not occur due to the absence of the
360 viral envelope. VCC are often observed in proximity to the viral synapse that forms between an
361 infected and a target cell (Duncan et al., 2014; Gousset et al., 2008), where they potentially
362 participate in direct viral transmission. Interestingly, direct transmission of HIV-1 from macrophages
363 to $CD4^+$ T cells is inhibited by jasplakinolide (Duncan *et al.*, 2014), suggesting that the same actin-
364 dependent mechanisms that regulate VCC trafficking for viral release, also impact its redistribution
365 towards viral synapses. It would be valuable to explore whether the factors described in this work as
366 regulating viral release and VCC trafficking, such as PYK2 or the VCC coats, also play a role in cell-to-
367 cell HIV transmission.

368 To conclude, whether at the steady-state or upon a stimulus that requires sudden and drastic
369 changes in macrophage morphology, VCC appear to be dynamic structures that traffic through the
370 cell in a manner that depends on its associated actin and microtubule cytoskeleton (Gaudin et al.,
371 2012). In tissues, macrophages are constantly subjected to mechanical constraints as they navigate
372 through crowded tissues, in a manner dependent on cytoskeletal dynamics. Our work suggests that
373 HIV may exploit the macrophage biology to promote its own release and propagation.

374 **Material and Methods**

375

376 Cells

377 Plasmapheresis residues from healthy adult donors were obtained from the Établissement Français
378 du Sang (Paris, France). All donors signed informed consent allowing the use of their blood for
379 research purposes. Peripheral blood mononuclear cells (PBMC) were separated using Ficoll-Paque
380 (GE Healthcare), and monocytes were isolated by positive selection using CD14+ magnetic beads
381 (Miltenyi Biotec) and differentiated into macrophages for 7 days in RPMI (Gibco, Life Technologies)
382 supplemented with 5% fetal calf serum (FCS; Gibco), 5% human serum AB (Sigma), penicillin-
383 streptomycin (Gibco), and 25 ng/ml macrophage colony-stimulating factor (M-CSF; Miltenyi Biotec).

384 HeLa and HEK 293 FT cells were maintained by bi-weekly subpassage in DMEM (Gibco, Thermofisher
385 Scientific), supplemented with FCS and antibiotics.

386

387 Virus production and monocyte transduction with LifeAct-mCherry

388 Viral particles were produced by transfection of 293FT cells in 6-well plates with 3 µg of total DNA
389 and 8 mL TransIT-293 Transfection Reagent (Mirus Bio) per well. Plasmid mixes to produce HIV-1
390 viral particles consisted of 0.4 µg CMV-VSVG (pMD2.G; 12259; Addgene) and 2.6 µg of HIV proviral
391 plasmid. To quantify viral release we preferentially used viral particles produced from pNL-ΔENV-
392 VSVG which was kindly provided by O. Schwartz (Institut Pasteur, Paris, France). For examination of
393 the VCC by microscopy we employed the pNL-GAG-iGFP-ΔENV-VSVG, a viral construct in which EGFP
394 is placed between viral protease cleaving sites and between the matrix and capsid domains of Gag
395 (Hubner et al., 2007). Media was renewed 16 hours later, and viruses were harvested at around 48
396 hours after transfection, filtered through a 0.45 µm pore and stored at -80°C until use. Thawed viral
397 stocks were titrated by infecting the GHOST X4R5 reporter cell line.

398 A similar protocol was followed to produce lentiviral particles for monocyte transduction with Lifeact
399 m-cherry. Here, transfection mixes consisted of 0.4 µg CMV-VSVG, 1.0 µg of the packaging plasmid
400 PSPAX2 (12260; Addgene) and 1.6 µg of LifeAct-mCherry lentivector (pCDH1-CMV-LifeAct-mCherry).
401 In parallel, VPX-containing SIV particles were produced by transfecting 293FT cells with 0.4 µg CMV-
402 VSVG and 2.6 µg of pSIV3^{+} plasmid (Mangeot et al., 2000). Monocytes were transduced with equal
403 volumes of freshly harvested LifeAct-mCherry and SIV3 lentiviral particles in the presence of 8 µg/mL
404 of protamine (Sigma). At 48 hours, differentiating MDMs were exposed to 2 µg/mL of puromycin to

405 select for successfully transduced cells, and were harvested for experiments at day 7 of
406 differentiation.

407

408 *In vitro* infections and cell treatments

409 MDMs were infected with HIV-1 NL-GAG-iGFP-ΔENV-VSVG or NL-ΔENV-VSVG at a MOI of 1.0. After
410 16 hours, culture media was renewed, and the infection allowed to progress for further 72 hours. At
411 day 4 after infection, cells were exposed to the drugs or vehicle (DMSO) at concentrations and for
412 the time periods indicated in figure legends. Jasplakinolide (Sigma); CK666 (Sigma); Blebbistatin
413 (Sigma); Mycalolide B (Enzo Life Sciences); PF431396 (Tocris).

414 HeLa cells were infected with NL-ΔENV-VSVG at a MOI=1.0. After 16 hours, the culture media was
415 renewed, and the same drugs added at similar concentrations.

416 To assess the membrane connectivity of the VCC, we employed the CellBrite Fix membrane stain.
417 Briefly, infected MDMs were rinsed in PBS and incubated for 15 min at 37°C with a 1/1000 dilution
418 of CellBrite Fix-640 (Biotium). Cells were rinsed twice with PBS and fixed in PFA 4% for confocal
419 microscopy.

420 To assess the accessibility of VCC to anti-CD44 antibodies, infected MDMs were rinsed in PBS and
421 stained with anti-CD44 antibodies at RT for 15 mins, before rinsing twice with PBS and fixation with
422 PFA 4%. Cells were subsequently processed for confocal microscopy as described below.

423

424 Macrophage Micropatterning

425 We employed a deep UV light-based method to imprint micropatterns onto glass coverslips. 12-mm
426 coverslips were plasma treated and incubated with a solution of 0.1 mg/mL of poly(acrylamide)- g -
427 (PEG, 1,6-hexanediamine,3-aminopropyldimethylethoxysilane, (PAcrAm-g-(PEG, NH2, Si), Surface
428 Solutions, Zurich) (Serrano et al., 2016) in 10 mM HEPES pH=7.4. A quartz mask containing the
429 transparent motives for micropatterning was thoroughly washed with 70% ethanol, and coverslips
430 were attached to its quartz surface using a small volume of water. The mask was then subjected to
431 deep UV illumination in an UV ozone oven (UVO cleaner, model 342-220, Jelight) for 10 min into its
432 silver face to induce degradation of PEG chains in the coverslips accessible through the transparent
433 motives. Coverslips were finally detached from the mask and incubated for 1 hour at RT with a 5
434 µg/mL solution of fibronectin (Sigma) in NaHCO3 100 mM. MDMs, previously infected with HIV-1 NL-
435 GAG-iGFP-ΔENV-VSVG (MOI=1.0) for 3 days, were seeded over patterned coverslips (20000 cells per

436 coverslip) in pre-warmed media and allowed to attach for 1 hour at 37°C. Non-adherent cells were
437 washed by media changes and the adherent cells were fixed in PFA 4%.

438

439 Frustrated Phagocytosis

440 Twelve mm glass coverslips were extensively washed with 70% ethanol, dried and incubated with 10
441 μg/mL of IgG from human serum (Sigma) in PBS for 1 hour at RT. For quantification of p24 release,
442 24-well culture plates were directly coated with human IgG. MDM were infected with HIV-1 NL-GAG-
443 iGFP-ΔENV-VSVG for microscopy, or with HIV-1 NL-ΔENV-VSVG for p24 quantification at a MOI=1.0.
444 At day 3 after infection, cells were detached, washed and seeded over IgG-coated substrates (5000
445 cells for microscopy, 20000 for p24 quantification). Cells were subsequently fixed in PFA at 30 mins
446 for fixed cell confocal microscopy, or immediately imaged for live cell imaging. For p24 release
447 quantification, aliquots of the supernatant were collected at the indicated time-points, filtered
448 (0.45μm) to remove floating cells, and stored until quantification by the p24 CBA.

449

450 Quantification of p24 in culture supernatant or cell lysates by cytometric bead array (CBA)

451 Culture supernatant or cell pellets were lysed in a buffer containing 0.1% BSA, 1% NP-40 and 0.02%
452 Tween-20. The amount of p24 in samples was subsequently quantified by a custom-made CBA assay
453 that detects the HIV-1 p24 protein. Briefly, B6 functional beads (BD Biosciences) were conjugated
454 with an anti-GAG antibody (H183-H12-5C hybridoma (mouse IgG1), NIH) and serve as capturing
455 beads by incubation with samples for 1 hour at room temperature with agitation. An anti-p24
456 detection antibody (KC57-FITC, Beckmann Coulter) is subsequently added and incubated for 2 hours
457 at RT. After two washes in a buffer containing 0.1% NP-40, beads are flowed in a FACS Verse (BD
458 Biosciences) and the p24 concentration in culture estimated using a standard curve with serial
459 dilutions of recombinant p24. For cell lysates an aliquot of the sample was used to quantify total
460 protein by the BCA method (Pierce Micro BCA kit, Thermo Fisher Scientific) and the data is presented
461 as μg of p24 / mg of total cell protein.

462

463 Western Blot

464 Cells were lysed in RIPA buffer and total protein levels quantified with the BCA method. 30 μg of
465 sample was reduced with Laemmli buffer, boiled and loaded in pre-cast polyacrylamide gels
466 (BioRad). After transfer onto PDVF membranes (BioRad), blocking buffer (5% non-fat dry milk (m/v)
467 in PBS-Tween-20 0.1% (v/v)) was added for 1 hour at RT. Primary antibodies were added overnight

468 at 4°C with gentle agitation in antibody dilution buffer (5% BSA in PBST), washed and incubated with
469 species-matched secondary HRP-conjugated secondary antibodies for 1 hour at RT. Membranes
470 were revealed in a BioRad Chemidoc after addition of HRP substrate (Clarity, Biorad). Densitometry
471 quantifications were performed using the ImageLab software (BioRad).

472

473 Confocal microscopy and Immunostaining

474 Cells were fixed in 4% paraformaldehyde (PFA), washed in PBS and then permeabilized with
475 permeabilization buffer (BSA 1% (m/v), Triton X-100 0.3% (v/v) in PBS) for 1 hour at room
476 temperature. The primary antibodies used were anti-F-actin, anti-CD18, anti-pPYK2 and anti-CD44,
477 as listed in supplementary table 1. Primary antibodies were diluted in permeabilization buffer, and
478 the staining was performed overnight at 4°C in the dark. Subsequently, cells were washed 3 times
479 and secondary staining was done in permeabilization buffer supplemented with 5% Donkey serum
480 (Sigma) for 1 hour. For secondary antibodies, donkey anti-rabbit A647 or donkey anti-mouse Alexa
481 647 (Invitrogen) were used. Phalloidin-AF647 (Invitrogen) staining was also performed at this stage.
482 Cells were washed 3 times then rinsed in PBS and mounted in Fluoromont-GTM medium with DAPI
483 (Invitrogen).

484 Cell imaging was performed on an inverted confocal microscope (Leica DMi8, SP8 scanning head
485 unit) equipped with a 63x oil immersion objective (NA=1.4) and four laser diodes (405, 488, 546, and
486 633 nm). An optimized z-step of 0.31 µm was employed for all acquisitions.

487

488 Image analysis and quantification

489 Image J was used for all image analyses and quantifications, using custom-made macro scripts to
490 automate the analysis. The Gag-iGFP signal was used to define a binary mask on the VCC, at each z-
491 slice. The total volume of the VCC was then obtained by summation of the binary mask value, at
492 each x,y pixel, across all the z-stack, correcting for the known dimensions of the voxel. A similar
493 strategy was employed to estimate the total cell volume. Depending on the staining, the binary
494 masks to define the cell area at each z-slice were derived from the phalloidin, F-actin or CD18
495 staining. Mean Gag intensity corresponds to the average Gag-iGFP signal at the region defined as
496 the VCC by the binary mask.

497 To calculate VCC dispersion (spreading) across the cell, we used maximum intensity projections of
498 the VCC's binary mask and determined its centroid. Spreading was then determined by calculating
499 the average distance of each VCC's pixel in the projected mask to the centroid. A similar strategy was

500 used to calculate the average distance of the VCC to the nuclear centroid. In this case, DAPI was used
501 to define the nuclear binary mask, which after maximum intensity projection, was used to determine
502 its centroid.

503 To determine the enrichment of CD18, p-PYK2 or CellBrite at the VCC, we first defined the VCC and
504 cell binary masks and obtained the average intensity for the CD18, p-PYK2 or CellBrite staining in
505 both the VCC and the whole cell. The enrichment score was then obtained as the ratio between the
506 average intensity at the VCC and the average intensity in the whole cell.

507 All image montages were assembled using ImageJ. Y-projections were obtained using the Reslice
508 tool, followed by maximum intensity projections. The 3D reconstructions which were achieved by
509 applying the Volume Viewer plugin to the binary masks of the channels imaged.

510

511 Live cell imaging

512 For live imaging experiments, cells were imaged on an inverted confocal microscope (Leica DMi8,
513 SP8 scanning head unit) equipped with a 40X oil immersion objective and a live cell imaging chamber
514 to maintain a constant temperature of 37°C and CO2 levels of 5%.

515 To assess the dynamics of the actin cytoskeleton surrounding the VCC, MDMs transduced with
516 lifeact-mCherry were infected with HIV-1 GAG-iGFP ΔENV-VSVG at a MOI=1.0 for 6 days in glass
517 bottom 35-mm dishes (Ibidi). Z-stacks were acquired in real-time at a frame rate of 0.42/s.

518 To image infected MDMs during frustrated phagocytosis, cells were placed in the imaging chamber
519 immediately after their addition to IgG-coated 35-mm glass bottom disks. Z-stacks were acquired at
520 a frame rate of 0.041/s. Acquired images were processed in ImageJ to assemble videos and
521 montages.

522

523 Electron microscopy

524 MDMs infected with HIV-1-NL-ΔENV-VSVG, were fixed in 2% glutaraldehyde in 0.1 M cacodylate
525 buffer, pH 7.4 for 1 hour and subsequently fixed for 1 hour in 2% buffered osmium tetroxide,
526 dehydrated in a graded series of ethanol solution, and then embedded in epoxy resin. Images were
527 acquired with a digital camera Quemesa (SIS) mounted on a Tecnai Spirit transmission electron
528 microscope (FEI) operated at 80 kV.

529

530 Statistical analysis

Data were analysed using Prism software v9 (GraphPad). If not specified in figure legends, graphics show individual donors as dots with bars or lines at the means. Distributions were assumed to be non-parametric, and the specific test employed is indicated at the figure legend. ns, P value of >0.05; *, P value of ≤0.05; **, P value of ≤0.01; ***, P value of ≤0.001; ****, P value of ≤0.0001.

Acknowledgements

We thank Dr Claire Hivroz and Ana-Maria Lennon-Dumenil at Institut Curie for fruitful discussions and critical reading of the manuscript. We also thank François-Xavier Gobert and Nicolas Carpi for discussions or technical help. This work was supported by grants from Agence Nationale de Recherche contre le SIDA et les hépatites virales (ANRS), Ensemble contre le SIDA (Sidaction), Laboratoire d'Excellence (Labex) DCBIOL (ANR-10-IDEX-0001-02 PSL and ANR-11-LABX-0043) to P.B. V.R. was supported by fellowships from ANRS and Sidaction.

Author Contributions

VR, PB and MM designed the research. VR, ST, MSR, EG and AH performed the research. VR, ST, MM and MSR analysed the data. VR and PB supervised research. VR, ST and PB wrote the paper.

547 **Figure Legends**

548

549 **Figure 1.** Actin is involved in VCC dynamics and viral release from macrophages

550 **A** – MDM infected with HIV-1 GAG-iGFP-ΔENV-VSVG for 7 days, stained for phalloidin. Scale bar = 30
551 µm. The bottom panel shows a maximum intensity z-projection. The top panel shows a slice on the
552 xz plane, highlighting the selected region for panel 1B.

553 **B** – Maximum intensity Z projection and 3D volume rendering of the region highlighted in 1A. Scale
554 bar = 1 µm

555 **C** – MDMs transduced with Lifeact-mCherry were infected with HIV-1-GAG-iGFP-dENV-VSVG
556 (MOI=1.0). Time-lapse imaging was performed at day 6 after infection. The bottom panels represent
557 the dashed region in the top panels. Scale bar= 20um (top panels) and 5um (bottom panels)

558 **D** – MDMs were infected with HIV-1-ΔENV-VSVG at a MOI=1.0 for 4 days. Cells were subsequently
559 treated with the indicated drugs for 24 hours. Supernatant aliquots were recovered at the indicated
560 time-points, and the released p24 was quantified by a custom-made CBA assay. Jasplakinolide = 50
561 nM / CK666 = 10 µM / Blebbistatin = 5 µM / Mycalolide-B = 100 nM. Data from 3 independent
562 donors. Two-way ANOVA. *= P<0.05

563 **E** – As in (D), cells were lysed at the end of the experimental procedure in NP-40 lysis buffer and
564 intracellular p24 was quantified by CBA. Data from 3 independent donors. One-Way ANOVA – (** =
565 P<0.01; *** P<0.001).

566 **F** – As in (D), cells were lysed in RIPA buffer at the end of the experimental procedure and analysed
567 by western blot for the expression of GAG. One representative donor is shown.

568 **G** – Densitometry quantification of the western blot bands from (F) for 3 independent donors. Paired
569 t-test, * = P<0.05, ns- non-significant

570

571 **Figure 2**. Stabilization of actin fibres scatters the VCC and increases the total volume of the
572 compartment

573 **A** – MDMs were grown in coverslips, infected with HIV-1-ΔENV-GAG-iGFP-VSVG at a MOI=1.0 for 4
574 days and subsequently treated with DMSO or jasplakinolide (100 nM) for 24 hours. Cells were fixed,
575 stained with anti-F-actin and imaged by confocal microscopy.

576 **B-E** – Image analysis for cells processed as in (A) for the indicated parameters. See methods for
577 details on the quantification strategies employed. Each circle represents one cell and the plots
578 display cells from 3 independent donors. Unpaired t-test. (** = $P<0.01$; ****$P<0.0001$).

579 **F** – Cells were treated as in (A) and processed for electron microscopy. The right panels are
580 enlargements of the areas enclosed in the dashed squares on the left panels. Scale bar = 2 µm (left
581 panels), 1 µm (right panel).

582

583 **Figure 3**. Stabilization of actin fibres relocalizes the integrin CD18 away from the VCC limiting
584 membrane in HIV-1-infected macrophages

585 **A-B** – MDMs were infected HIV-1-ΔENV-VSVG (MOI=1.0) for 7 days. Cells were fixed and processed
586 for electron microscopy. (A) depicts an example of an internal VCC with associated electron dense
587 coats. (B) highlights the presence of compartments with coats close to the cell surface. Arrow heads
588 point to the electron dense coats. Scaler bars= 2 µm.

589 **C** – Confocal microscopy of MDMs infected with HIV-1-Gag-iGFP-ΔENV-VSVG (MOI=1.0) for 4 days
590 and treated with jasplakinolide or DMSO for 24 hours. Whole cell projections are shown in the right,
591 along the z-axis (bottom) or the y axis (top). On the left, the areas enclosed in the dashed squares
592 are enlarged and shown as z-projections. Scale bar = 20 µm (left panels) or 2 µm (right panels).

593 **D** – Quantification of CD18 enrichment at the VCC by image analysis. Each dot represents a single
594 cell from 3 independent donors. See Methods for details on the analysis.

595 **E – F** - Electron microscopy of MDMs infected with HIV-1-ΔENV-VSVG (MOI=1.0) for 4 days and
596 treated with jasplakinolide or DMSO for 24 hours. Arrow heads point to electron dense regions
597 associated with the VCC in DMSO treated cells (note their absence in cells treated with
598 jasplakinolide). Scale bars= 2 µm.

599

600 **Figure 4**. The phosphorylated form of integrin-associated kinase PYK2 partially colocalizes with the
601 VCC

602 **A** – MDMs left uninfected or infected with HIV-1-Δ-ENV-VSVG (MOI=1.0) for 4 days were treated
603 with jasplakinolide or vehicle (DMSO) for 24 hours. Cells were lysed and analysed by western blot for
604 the indicated proteins. The higher concentration of Jasplakinolide employed was 200 nM and the
605 lower concentrations correspond to consecutive two-fold dilutions.

606 **B** – Confocal microscopy of MDMs infected with HIV-1-Gag-iGFP-ΔENV-VSVG (MOI=1.0) for 4 days
607 and treated with jasplakinolide or DMSO for 24 hours. Whole cell projections are shown on the right,
608 along the z-axis (bottom) or the y axis (top). On the left, the areas enclosed in the dashed squares
609 are enlarged and shown as z-projections. Scale bar = 20 µm (left panels) or 2 µm (right panels).

610 **C** – Quantification of P-(Y402)-PYK2 enrichment at the VCC by image analysis. Each dot represents a
611 single cell from 2 independent donors. See Methods for details on the analysis.

612

613 **Figure 5**. A PYK2 inhibitor promotes HIV-1 retention in VCC

614 **A** – MDMs left uninfected or infected with HIV-1-Δ-ENV-VSVG (MOI=1.0) for 4 days were treated
615 with PF396 or vehicle (DMSO) for additional 96 hours. Cells were lysed and analysed by western blot
616 with the indicated antibodies. The table below the blots display the intensity ratios indicated, as
617 measured by densitometry.

618 **B** – MDMs were infected with HIV-1-ΔENV-VSVG at a MOI=1.0 for 4 days. Cells were subsequently
619 treated with PF396 (1µM). At the indicated time-points, supernatant aliquots were recovered, and
620 the released p24 was quantified by CBA. Data from 3 independent donors. Two-way ANOVA. *=
621 $P<0.05$

622 **C** – As in (B), cells were lysed at the end of the experimental procedure in NP-40 lysis buffer and
623 intracellular p24 was quantified by CBA. Data from 3 independent donors. Paired t test – (** =
624 $P<0.01$).

625 **D** – Confocal microscopy of MDMs infected with HIV-1-Gag-iGFP-ΔENV-VSVG (MOI=1.0) for 4 days
626 and treated with PF396 (1µM) or vehicle (DMSO) for an additional 96 hours. Whole cell projections
627 are shown on the right, along the z-axis (bottom) or the y axis (top). On the left, the areas enclosed
628 in the dashed squares are zoomed in and shown as z-projections. Scale bar = 20 µm (left panels) or 2
629 µm (right panels).

630 **E-H** – Image analysis for cells processed as in (D) for the indicated parameters. See methods for
631 details on the quantification strategies employed. Each circle represents one cell, and the plots show
632 cells from 3 independent donors. Unpaired t-test. (* = $P<0.05$; *** $P<0.001$).

633 **I -** CD18 enrichment at the VCC for cells processed as in Fig. S4. See methods for details on image
634 analysis. Each circle represents one cell, and the plots display cells from 2 independent donors.
635 Unpaired t-test. (ns= not significant).

636 **J** – Confocal microscopy of MDMs infected with HIV-1-Gag-iGFP-ΔENV-VSVG (MOI=1.0) for 4 days
637 and treated with PF396 (1µM) or vehicle (DMSO) for additional 96 hours. Cells were exposed to

638 CellBrite before fixation. Right panel - whole cell projections along the z-axis (bottom) or the y axis
639 (top). Left, panels – magnification of the areas enclosed in the dashed squares as z-projections. Scale
640 bar = 20 µm (left panels) or 2 µm (right panels).

641 **K-L** – Quantification of CellBrite intensity in the VCC (L) or elsewhere in the cell (M) for cells
642 processed as in (K). See methods for details. Each circle represents one cell, and the plots show cells
643 from 2 independent donors. Unpaired t-test. (Ns-non-significant; *** *P*<0.001).

644

645 **Figure 6**. Rapid HIV release during macrophage frustrated phagocytosis is associated with trafficking
646 of $CD18^+$ VCC to the surface

647 **A** – Time-lapse imaging of MDMs infected with HIV-1-GAG-iGFP-ΔENV-VSVG for 3 days and seeded
648 over human IgG-coats coverslips. Whole cell projections are shown for the top and middle panels,
649 along the z-axis (middle) or the y axis (top). The bottom panel (transmission channel) is a single z-
650 slice. Scale bar = 20 µm.

651 **B** – Image analysis of the total VCC volume (left y-axis) and the cell projected area (right y-axis) over
652 the course of the frustrated phagocytosis event depicted in (A).

653 **C** – MDMs infected with HIV-1-ΔENV-VSVG for 3 days were seeded over human IgG-coated
654 coverslips, or over non-coated coverslips, or in the presence of soluble IgG over non-coated
655 coverslips. At the indicated time-points, aliquots of the supernatant were recovered and the
656 released p24 was quantified by CBA. Data from 3 independent donors. For each time-point groups
657 were compared by one-way ANOVA (* = *P*<0.05).

658 **D** – Confocal microscopy of MDMs infected with HIV-1-Gag-iGFP-ΔENV-VSVG (MOI=1.0) for 3 days
659 and seeded over control or human IgG-coated coverslips for 30 mins. Right panels - whole cell
660 projections along the z-axis (bottom) or the y axis (top). Left, panels – magnification of the areas
661 enclosed in the dashed squares as z-projections. Scale bar = 20 µm (left panels) or 2 µm (right
662 panels).

663 **E-H** – Image analysis for cells processed as in (D) for the indicated parameters. See methods for
664 details on the quantification strategies employed. Each circle represents one cell, and the plots
665 include cells from 2 independent donors. Unpaired t-test. (** = *P*<0.01; ****P*<0.0001).

666

667 **References**

668 Bear, J.E., and Haugh, J.M. (2014). Directed migration of mesenchymal cells: where signaling
669 and the cytoskeleton meet. Curr Opin Cell Biol *30*, 74-82. 10.1016/j.ceb.2014.06.005.
670 Berre, S., Gaudin, R., Cunha de Alencar, B., Desdouits, M., Chabaud, M., Naffakh, N., Rabaza-
671 Gairi, M., Gobert, F.X., Jouve, M., and Benaroch, P. (2013). CD36-specific antibodies block
672 release of HIV-1 from infected primary macrophages and its transmission to T cells. J Exp
673 Med *210*, 2523-2538. 10.1084/jem.20130566.
674 Chalut, K.J., and Paluch, E.K. (2016). The Actin Cortex: A Bridge between Cell Shape and
675 Function. Dev Cell *38*, 571-573. 10.1016/j.devcel.2016.09.011.
676 Chu, H., Wang, J.J., Qi, M., Yoon, J.J., Wen, X., Chen, X., Ding, L., and Spearman, P. (2012).
677 The intracellular virus-containing compartments in primary human macrophages are largely
678 inaccessible to antibodies and small molecules. PLoS One *7*, e35297.
679 10.1371/journal.pone.0035297.
680 Davis, C.B., Dikic, I., Unutmaz, D., Hill, C.M., Arthos, J., Siani, M.A., Thompson, D.A.,
681 Schlessinger, J., and Littman, D.R. (1997). Signal transduction due to HIV-1 envelope
682 interactions with chemokine receptors CXCR4 or CCR5. J Exp Med *186*, 1793-1798.
683 10.1084/jem.186.10.1793.
684 Del Corno, M., Liu, Q.H., Schols, D., de Clercq, E., Gessani, S., Freedman, B.D., and Collman,
685 R.G. (2001). HIV-1 gp120 and chemokine activation of Pyk2 and mitogen-activated protein
686 kinases in primary macrophages mediated by calcium-dependent, pertussis toxin-insensitive
687 chemokine receptor signaling. Blood *98*, 2909-2916. 10.1182/blood.v98.10.2909.
688 Deneka, M., Pelchen-Matthews, A., Byland, R., Ruiz-Mateos, E., and Marsh, M. (2007). In
689 macrophages, HIV-1 assembles into an intracellular plasma membrane domain containing
690 the tetraspanins CD81, CD9, and CD53. J Cell Biol *177*, 329-341. 10.1083/jcb.200609050.
691 Duncan, C.J., Williams, J.P., Schiffner, T., Gartner, K., Ochsenbauer, C., Kappes, J., Russell,
692 R.A., Frater, J., and Sattentau, Q.J. (2014). High-multiplicity HIV-1 infection and neutralizing
693 antibody evasion mediated by the macrophage-T cell virological synapse. J Virol *88*, 2025-
694 2034. 10.1128/JVI.03245-13.
695 Duong, L.T., and Rodan, G.A. (2000). PYK2 is an adhesion kinase in macrophages, localized in
696 podosomes and activated by beta(2)-integrin ligation. Cell Motil Cytoskeleton *47*, 174-188.
697 10.1002/1097-0169(200011)47:3<174::AID-CM2>3.0.CO;2-N.

698 Gaudin, R., Berre, S., Cunha de Alencar, B., Decalf, J., Schindler, M., Gobert, F.X., Jouve, M.,
699 and Benaroch, P. (2013). Dynamics of HIV-containing compartments in macrophages reveal
700 sequestration of virions and transient surface connections. PLoS One *8*, e69450.
701 10.1371/journal.pone.0069450.
702 Gaudin, R., de Alencar, B.C., Jouve, M., Berre, S., Le Bouder, E., Schindler, M., Varthaman, A.,
703 Gobert, F.X., and Benaroch, P. (2012). Critical role for the kinesin KIF3A in the HIV life cycle
704 in primary human macrophages. J Cell Biol *199*, 467-479. 10.1083/jcb.201201144.
705 Gousset, K., Ablan, S.D., Coren, L.V., Ono, A., Soheilian, F., Nagashima, K., Ott, D.E., and
706 Freed, E.O. (2008). Real-time visualization of HIV-1 GAG trafficking in infected macrophages.
707 PLoS Pathog *4*, e1000015. 10.1371/journal.ppat.1000015.
708 Graziano, F., Desdouits, M., Garzetti, L., Podini, P., Alfano, M., Rubartelli, A., Furlan, R.,
709 Benaroch, P., and Poli, G. (2015). Extracellular ATP induces the rapid release of HIV-1 from
710 virus containing compartments of human macrophages. Proc Natl Acad Sci U S A *112*,
711 E3265-3273. 10.1073/pnas.1500656112.
712 Hayashi-Takanaka, Y., Kina, Y., Nakamura, F., Yamazaki, S., Harata, M., Soest, R., Kimura, H.,
713 and Nakao, Y. (2019). Effect of mycalolides isolated from a marine sponge Mycale aff.
714 nullarosette on actin in living cells. Sci Rep *9*, 7540. 10.1038/s41598-019-44036-2.
715 Hubner, W., Chen, P., Del Portillo, A., Liu, Y., Gordon, R.E., and Chen, B.K. (2007). Sequence
716 of human immunodeficiency virus type 1 (HIV-1) Gag localization and oligomerization
717 monitored with live confocal imaging of a replication-competent, fluorescently tagged HIV-
718 1. J Virol *81*, 12596-12607. 10.1128/JVI.01088-07.
719 Ladinsky, M.S., Khamaikawin, W., Jung, Y., Lin, S., Lam, J., An, D.S., Bjorkman, P.J., and
720 Kieffer, C. (2019). Mechanisms of virus dissemination in bone marrow of HIV-1-infected
721 humanized BLT mice. Elife *8*. 10.7554/eLife.46916.
722 Mangeot, P.E., Negre, D., Dubois, B., Winter, A.J., Leissner, P., Mehtali, M., Kaiserlian, D.,
723 Cosset, F.L., and Darlix, J.L. (2000). Development of minimal lentivirus vectors derived from
724 simian immunodeficiency virus (SIVmac251) and their use for gene transfer into human
725 dendritic cells. J Virol *74*, 8307-8315. 10.1128/jvi.74.18.8307-8315.2000.
726 Masters, T.A., Pontes, B., Viasnoff, V., Li, Y., and Gauthier, N.C. (2013). Plasma membrane
727 tension orchestrates membrane trafficking, cytoskeletal remodeling, and biochemical
728 signaling during phagocytosis. Proc Natl Acad Sci U S A *110*, 11875-11880.
729 10.1073/pnas.1301766110.

730 Mlcochova, P., Pelchen-Matthews, A., and Marsh, M. (2013). Organization and regulation of
731 intracellular plasma membrane-connected HIV-1 assembly compartments in macrophages.
732 BMC Biol *11*, 89. 10.1186/1741-7007-11-89.
733 Okigaki, M., Davis, C., Falasca, M., Harroch, S., Felsenfeld, D.P., Sheetz, M.P., and
734 Schlessinger, J. (2003). Pyk2 regulates multiple signaling events crucial for macrophage
735 morphology and migration. Proc Natl Acad Sci U S A *100*, 10740-10745.
736 10.1073/pnas.1834348100.
737 Olazabal, I.M., Caron, E., May, R.C., Schilling, K., Knecht, D.A., and Machesky, L.M. (2002).
738 Rho-kinase and myosin-II control phagocytic cup formation during CR, but not FcgammaR,
739 phagocytosis. Curr Biol *12*, 1413-1418. 10.1016/s0960-9822(02)01069-2.
740 Orenstein, J.M., Meltzer, M.S., Phipps, T., and Gendelman, H.E. (1988). Cytoplasmic
741 assembly and accumulation of human immunodeficiency virus types 1 and 2 in recombinant
742 human colony-stimulating factor-1-treated human monocytes: an ultrastructural study. J
743 Virol *62*, 2578-2586. 10.1128/JVI.62.8.2578-2586.1988.
744 Ospina Stella, A., and Turville, S. (2018). All-Round Manipulation of the Actin Cytoskeleton
745 by HIV. Viruses *10*. 10.3390/v10020063.
746 Pelchen-Matthews, A., Giese, S., Mlcochova, P., Turner, J., and Marsh, M. (2012). beta2
747 integrin adhesion complexes maintain the integrity of HIV-1 assembly compartments in
748 primary macrophages. Traffic *13*, 273-291. 10.1111/j.1600-0854.2011.01306.x.
749 Rahman, S.A., Koch, P., Weichsel, J., Godinez, W.J., Schwarz, U., Rohr, K., Lamb, D.C.,
750 Krausslich, H.G., and Muller, B. (2014). Investigating the role of F-actin in human
751 immunodeficiency virus assembly by live-cell microscopy. J Virol *88*, 7904-7914.
752 10.1128/JVI.00431-14.
753 Rodrigues, V., Ruffin, N., San-Roman, M., and Benaroch, P. (2017). Myeloid Cell Interaction
754 with HIV: A Complex Relationship. Front Immunol *8*, 1698. 10.3389/fimmu.2017.01698.
755 Sattentau, Q.J., and Stevenson, M. (2016). Macrophages and HIV-1: An Unhealthy
756 Constellation. Cell Host Microbe *19*, 304-310. 10.1016/j.chom.2016.02.013.
757 Schaller, M.D. (2010). Cellular functions of FAK kinases: insight into molecular mechanisms
758 and novel functions. J Cell Sci *123*, 1007-1013. 10.1242/jcs.045112.
759 Serrano, A., Zurcher, S., Tosatti, S., and Spencer, N.D. (2016). Imparting Nonfouling
760 Properties to Chemically Distinct Surfaces with a Single Adsorbing Polymer: A Multimodal
761 Binding Approach. Macromol Rapid Commun *37*, 622-629. 10.1002/marc.201500683.

762 Thery, M. (2010). Micropatterning as a tool to decipher cell morphogenesis and functions. J
763 Cell Sci *123*, 4201-4213. 10.1242/jcs.075150.
764 Thomas, A., Mariani-Floderer, C., Lopez-Huertas, M.R., Gros, N., Hamard-Peron, E., Favard,
765 C., Ohlmann, T., Alcami, J., and Muriaux, D. (2015). Involvement of the Rac1-IRSp53-Wave2-
766 Arp2/3 Signaling Pathway in HIV-1 Gag Particle Release in CD4 T Cells. J Virol *89*, 8162-8181.
767 10.1128/JVI.00469-15.
768 Van Goethem, E., Poincloux, R., Gauffre, F., Maridonneau-Parini, I., and Le Cabec, V. (2010).
769 Matrix architecture dictates three-dimensional migration modes of human macrophages:
770 differential involvement of proteases and podosome-like structures. J Immunol *184*, 1049-
771 1061. 10.4049/jimmunol.0902223.
772 Verollet, C., Souriant, S., Bonnaud, E., Jolicoeur, P., Raynaud-Messina, B., Kinnaer, C.,
773 Fourquaux, I., Imle, A., Benichou, S., Fackler, O.T., et al. (2015). HIV-1 reprograms the
774 migration of macrophages. Blood *125*, 1611-1622. 10.1182/blood-2014-08-596775.
775 Welsch, S., Keppler, O.T., Habermann, A., Allespach, I., Krijnse-Locker, J., and Krausslich, H.G.
776 (2007). HIV-1 buds predominantly at the plasma membrane of primary human
777 macrophages. PLoS Pathog *3*, e36. 10.1371/journal.ppat.0030036.
778 Wen, X., Ding, L., Wang, J.J., Qi, M., Hammonds, J., Chu, H., Chen, X., Hunter, E., and
779 Spearman, P. (2014). ROCK1 and LIM kinase modulate retrovirus particle release and cell-
780 cell transmission events. J Virol *88*, 6906-6921. 10.1128/JVI.00023-14.
781 Zhu, X., Bao, Y., Guo, Y., and Yang, W. (2018). Proline-Rich Protein Tyrosine Kinase 2 in
782 Inflammation and Cancer. Cancers (Basel) *10*. 10.3390/cancers10050139.
783
784

785 **Figure 1.**

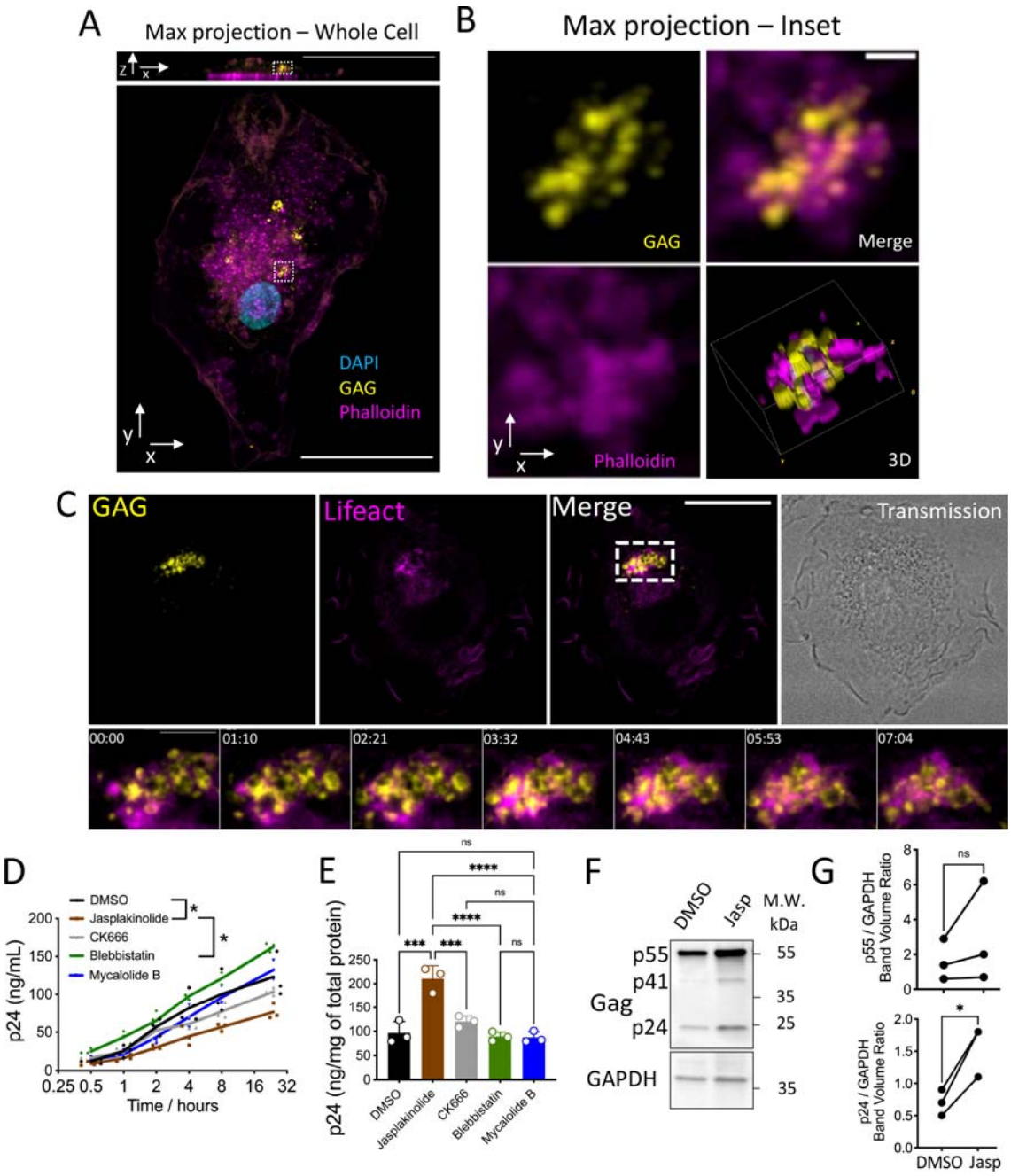

786

787

Figure 2.

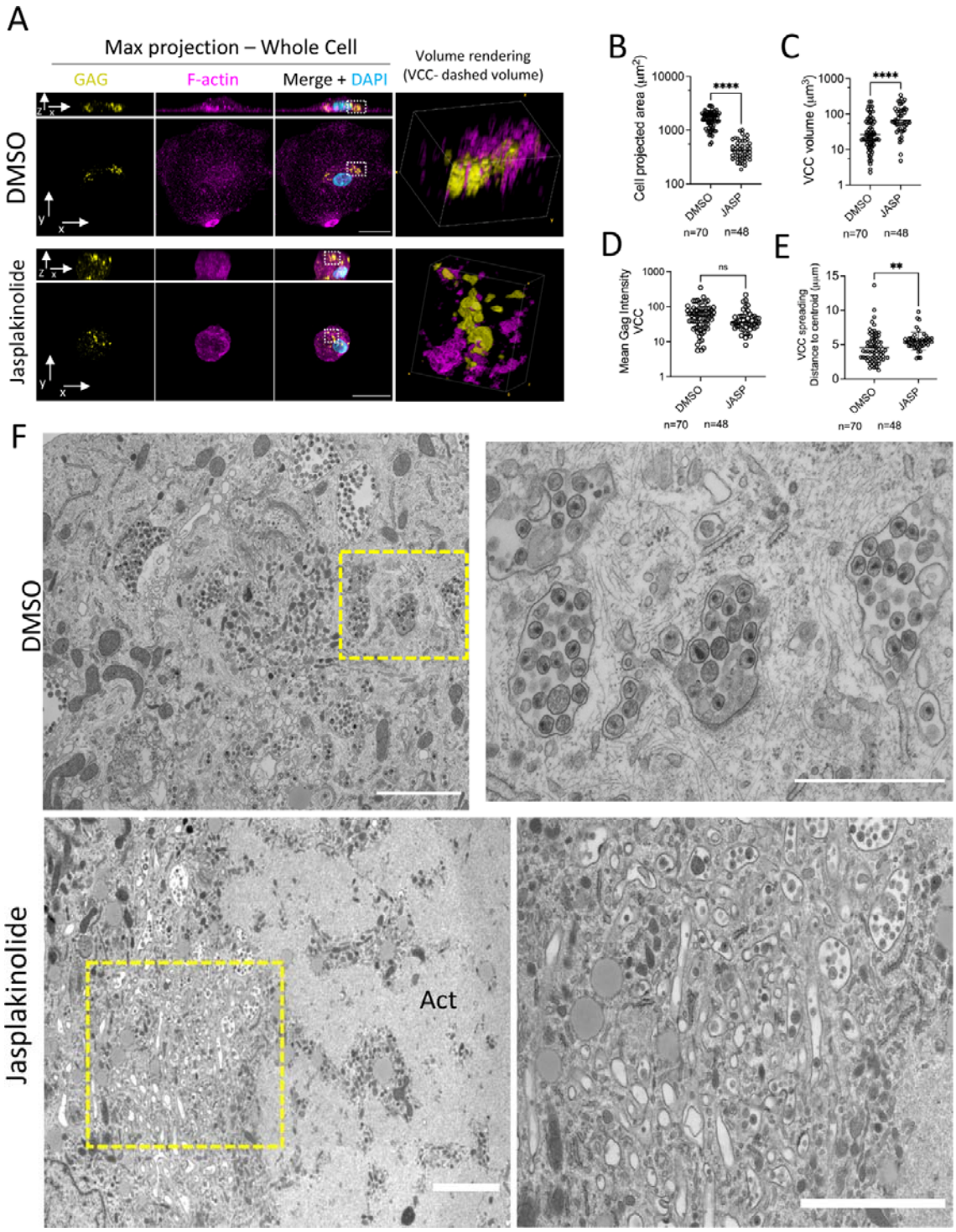
A
Max projection – Whole Cell
GAG
F-actin
Merge + DAPI
Volume rendering
(VCC- dashed volume)
DMSO
Jasplakinolide
B
Cell projected area (µm²)
10000
1000
100
****
DMSO
JASP
n=70
n=48
C
VCC volume (µm³)
1000
100
10
1
****
DMSO
JASP
n=70
n=48
D
Mean Gag Intensity VCC
1000
100
10
1
ns
DMSO
JASP
n=70
n=48
E
VCC spreading Distance to centroid (µm)
15
10
5
0
**
DMSO
JASP
n=70
n=48
F
DMSO
Jasplakinolide
Act

792 **Figure 3.**

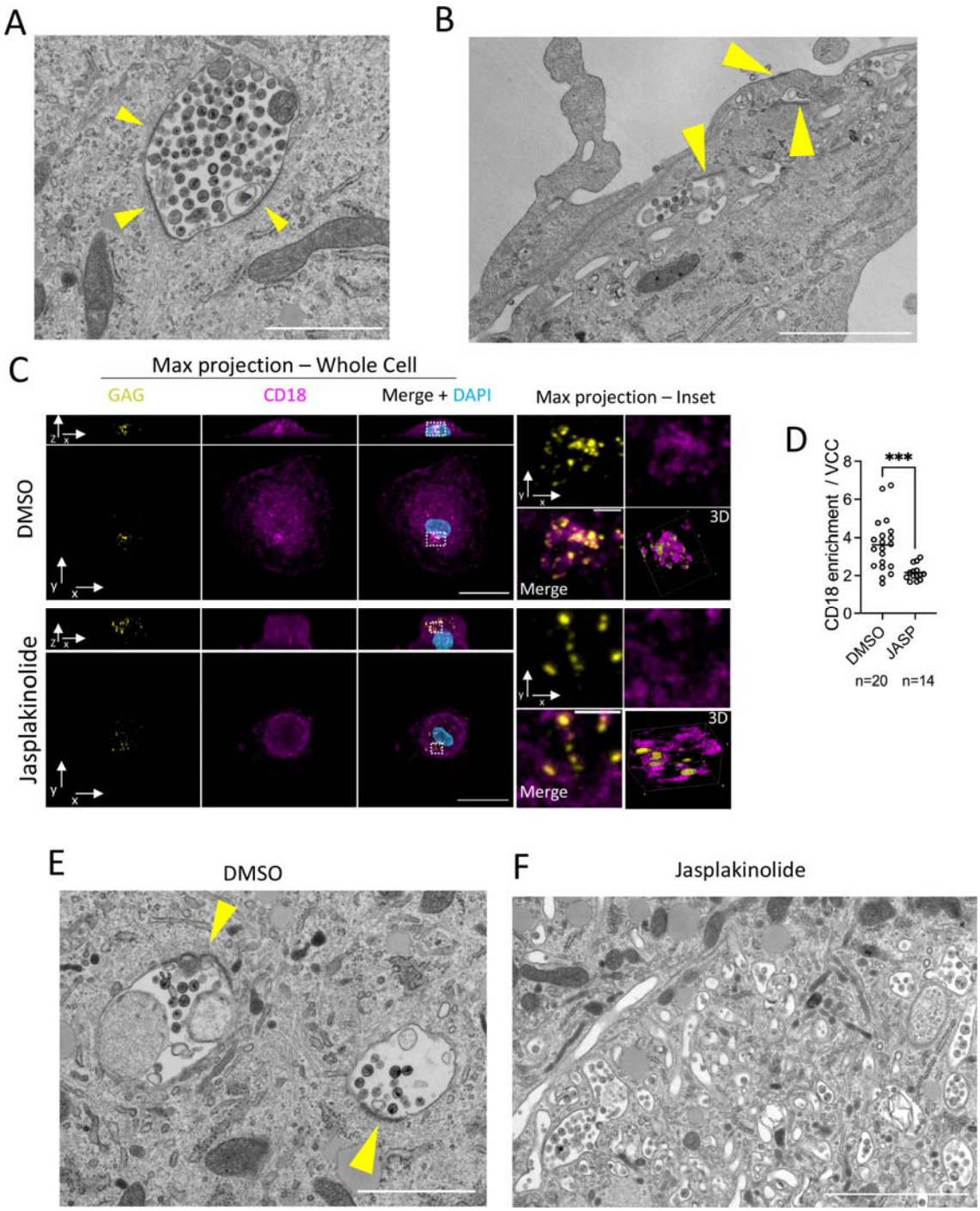

793

794

795

796

797

Figure 4.

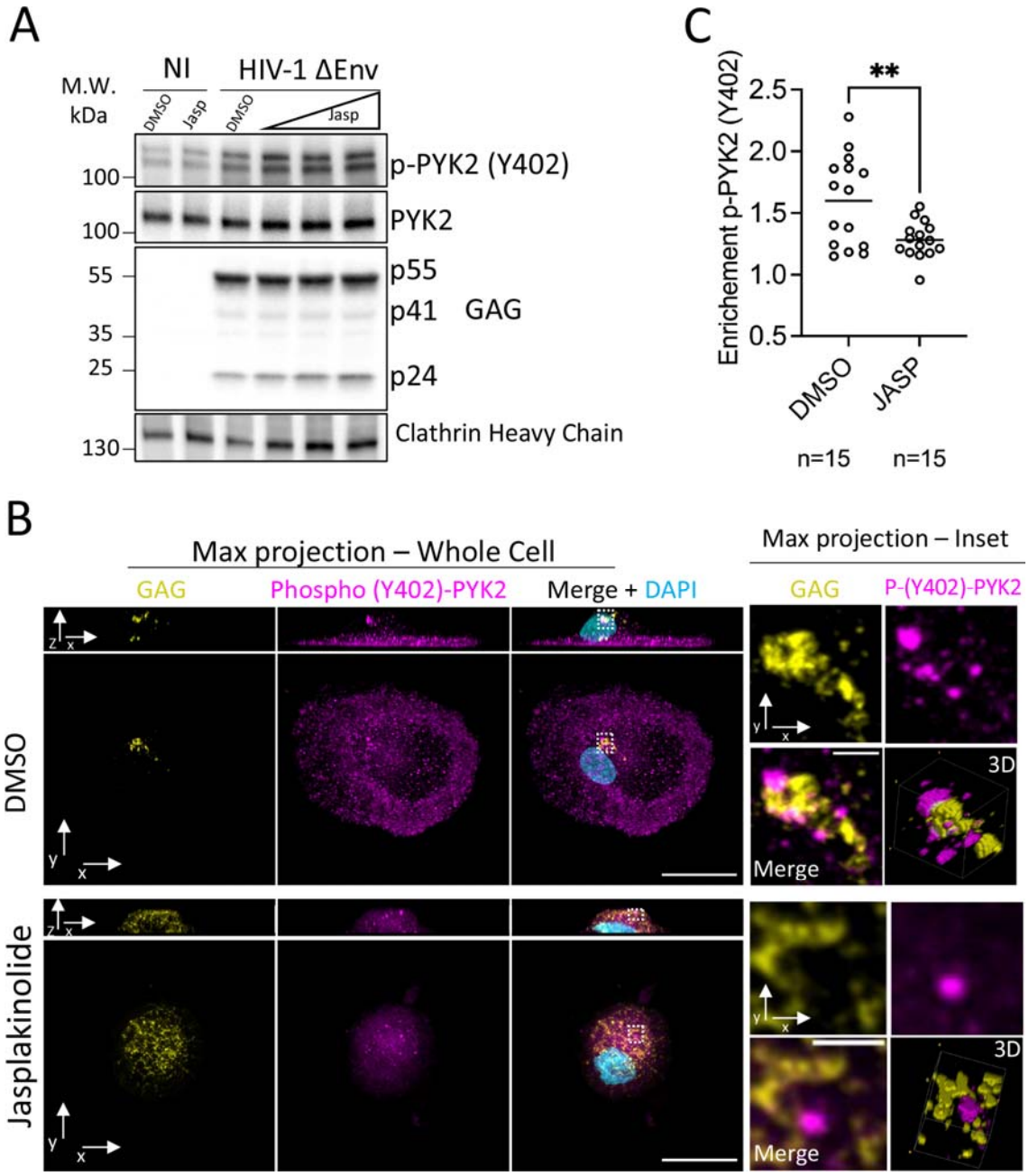
A
M.W.
kDa
NI
HIV-1 ΔEnv
DMSO
Jasp
DMSO
Jasp
100
100
55
35
25
130
p-PYK2 (Y402)
PYK2
p55
p41
GAG
p24
Clathrin Heavy Chain
C
Enrichement p-PYK2 (Y402)
2.5
2.0
1.5
1.0
0.5
**
DMSO
JASP
n=15
n=15
B
Max projection – Whole Cell
Max projection – Inset
GAG
Phospho (Y402)-PYK2
Merge + DAPI
GAG
P-(Y402)-PYK2
DMSO
Jasplakinolide
3D
Merge
3D
Merge

Figure 5.

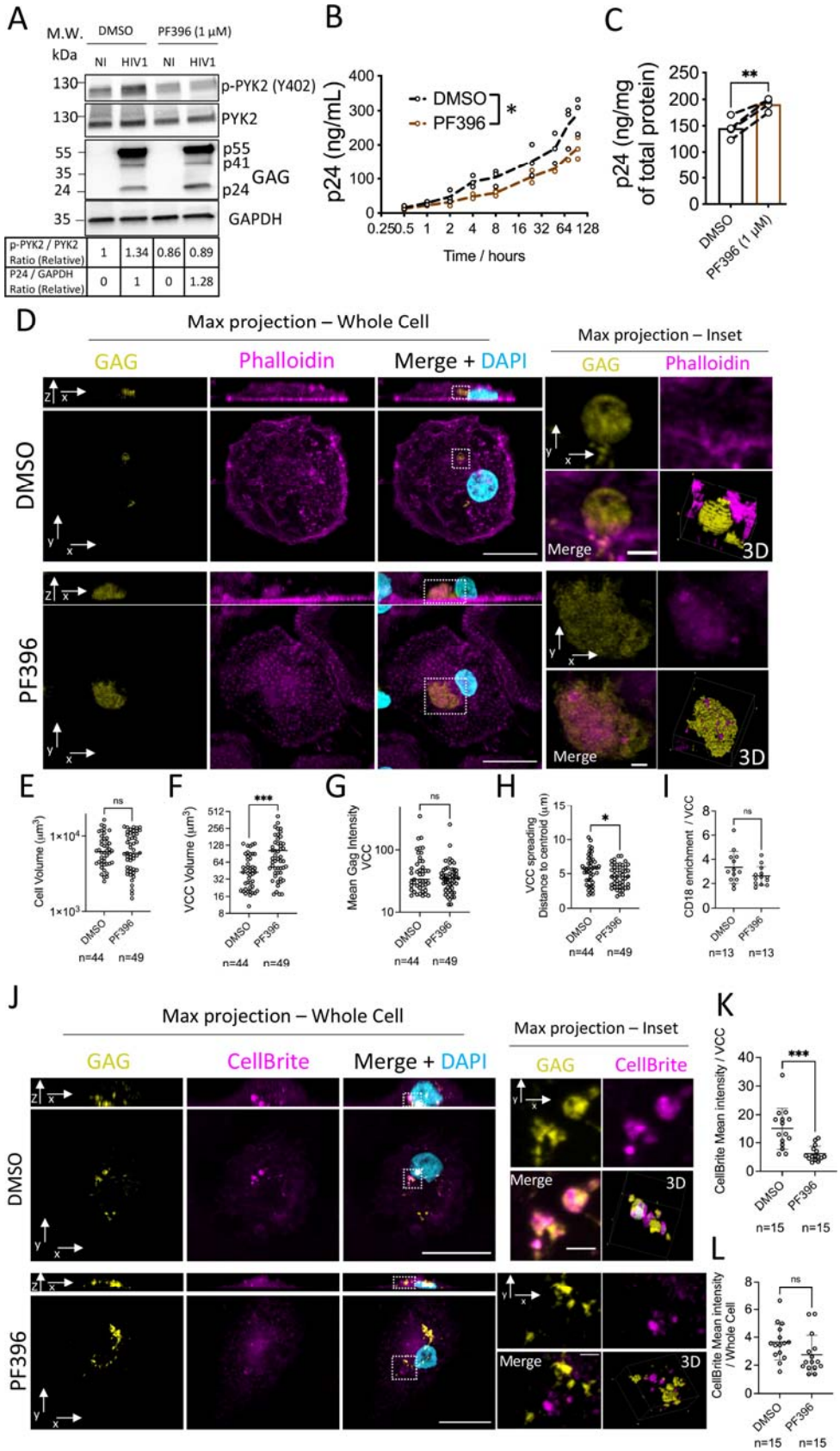
A
M.W. kDa
DMSO
PF396 (1 μM)
NI HIV1 NI HIV1
130
p-PYK2 (Y402)
130
PYK2
55
35
24
p55
p41
p24
GAG
35
GAPDH
p-PYK2 / PYK2 Ratio (Relative) 1 1.34 0.86 0.89
P24 / GAPDH Ratio (Relative) 0 1 0 1.28
B
p24 (ng/mL)
DMSO
PF396
*
Time / hours
C
p24 (ng/mg of total protein)
**
DMSO
PF396 (1 μM)
D
Max projection – Whole Cell
GAG
Phalloidin
Merge + DAPI
Max projection – Inset
GAG
Phalloidin
DMSO
PF396
Merge
3D
E
Cell Volume (μm³)
ns
DMSO PF396
n=44 n=49
F
VCC Volume (μm³)
***
DMSO PF396
n=44 n=49
G
Mean Gag Intensity VCC
ns
DMSO PF396
n=44 n=49
H
VCC spreading Distance to centroid (μm)
*
DMSO PF396
n=44 n=49
I
CD18 enrichment / VCC
ns
DMSO PF396
n=13 n=13
J
Max projection – Whole Cell
GAG
CellBrite
Merge + DAPI
Max projection – Inset
GAG
CellBrite
DMSO
PF396
Merge
3D
K
CellBrite Mean intensity / VCC
***
DMSO PF396
n=15 n=15
L
CellBrite Mean intensity / Whole Cell
ns
DMSO PF396
n=15 n=15

Figure 6.

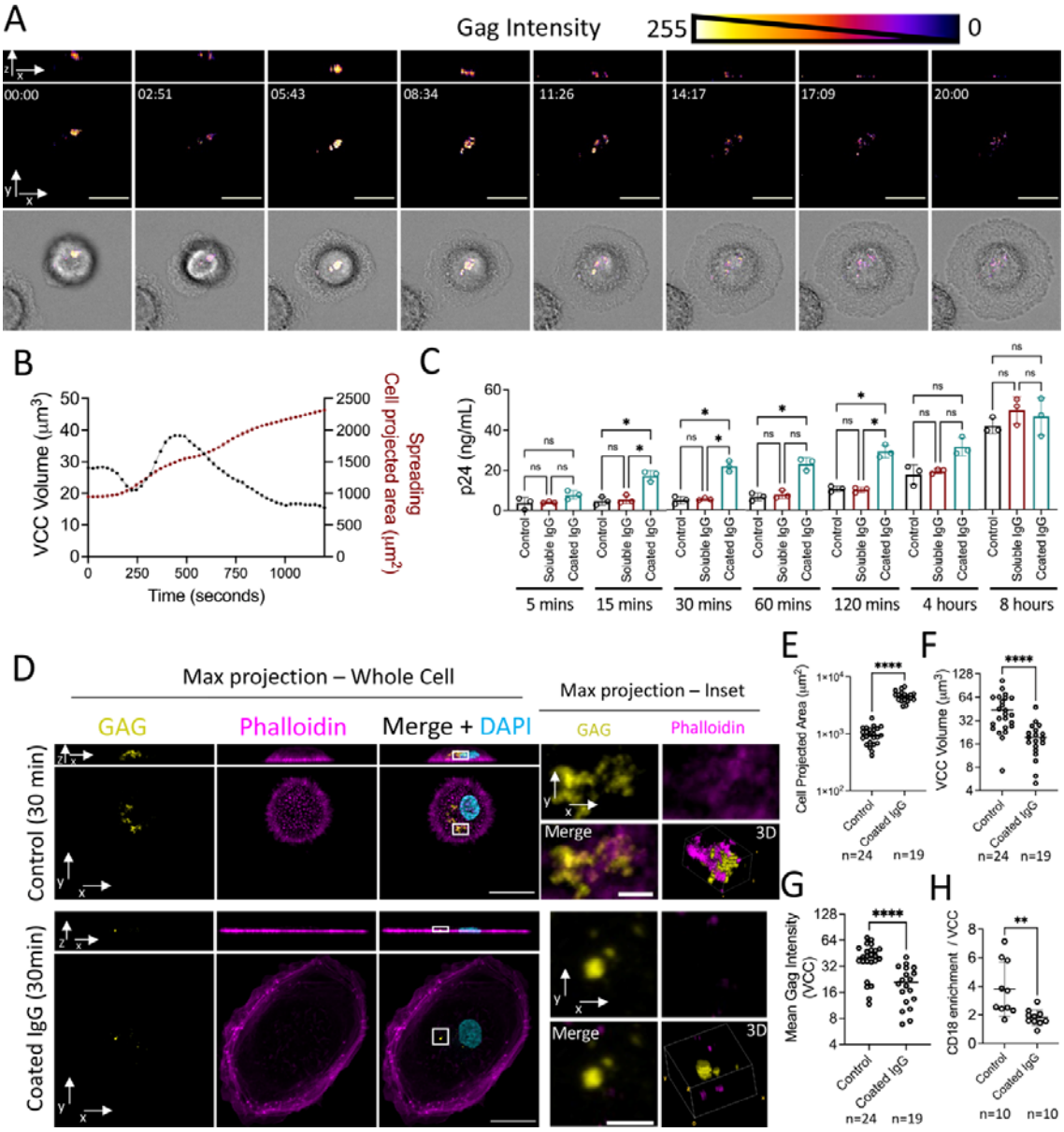
A
Gag Intensity
255
0
00:00
02:51
05:43
08:34
11:26
14:17
17:09
20:00
B
VCC Volume (μm³)
Cell projected area (μm²)
Spreading
Time (seconds)
C
p24 (ng/mL)
Control
Soluble IgG
Coated IgG
5 mins
15 mins
30 mins
60 mins
120 mins
4 hours
8 hours
D
Max projection – Whole Cell
Max projection – Inset
GAG
Phalloidin
Merge + DAPI
Merge
3D
Control (30 min)
Coated IgG (30min)
E
Cell Projected Area (μm²)
n=24
n=19
F
VCC Volume (μm³)
G
Mean Gag Intensity (VCC)
H
CD18 enrichment / VCC
n=10